J. Fluid Mech. (1984), *vol.* 140, *pp.* 303–327
Printed in Great Britain

Gravity current upstream of a buoyant influx in an open-channel flow: a numerical study

By DANIEL T. VALENTINE
Mechanical and Industrial Engineering Department, Clarkson College of Technology, Potsdam, New York 13676

AND TIMOTHY W. KAO
Civil Engineering Department, The Catholic University of America, Washington, DC 20017

(Received 25 July 1983)

The establishment of an upstream intrusion of a buoyant fluid discharged into an open-channel flow of uniform density and finite depth is studied numerically using the full Navier–Stokes and diffusion equations. The problem is posed as an initial-boundary-value problem for the laminar motions of a Boussinesq fluid. The equations are integrated numerically by finite-difference methods. The flow patterns produced are controlled by the influx of buoyancy; therefore they are characterized by an inflow densimetric Froude number. A comparison with available experimental data provides favourable support to the theoretical predictions. The critical value of densimetric Froude number of the source of a vertically downward inflow at the free surface of a channel is determined. For densimetric Froude number less than critical, an intrusion is established on the upstream side of the source. Because dissipative mechanisms associated with viscosity take a finite time to intervene, the intrusion starts as an inviscid gravity current with a propagation speed greater than the surface velocity of the stream. The front speed is proportional to the phase velocity of long internal waves. Subsequently, the front decelerates as the interfacial friction, and, if applicable, the boundary frictional forces increase simultaneously with mass entrainment across the interface. The current slows down towards a two-zone equilibrium: (1) the zone encompassing the current behind the frontal zone, where a steady state is approached with respect to the inertial frame of reference; (2) the frontal zone, where the upstream speed approaches a steady speed of frontal advance, albeit small. The upstream intrusion alters the flow pattern of the ambient stream dramatically. A significant feature of both the upstream and downstream currents is the presence of surface convergence with concomitant downwelling near the fronts. As the upstream front decelerates, wavelike disturbances are excited just behind the front at frequencies characteristic of internal waves. As the front approaches steady state, these disturbances appear to be damped. This problem has practical implications in the design of once-through cooling-water systems for power plants taking their cooling water from rivers.

1. Introduction

When an influx of buoyant fluid is introduced near the surface of an open-channel flow, a surface layer of the source fluid is formed. The buoyant surface layer spreads horizontally into the ambient stream; its motion is driven by gravitational forces interacting with inertial and viscous forces. When the appropriate conditions occur,

the surface layer intrudes upstream of the source location. Bata (1959) and Polk, Benedict & Parker (1971) reported field observations of upstream intrusions of the buoyant effluent of several power plants discharged into streams with relatively weak currents. The fully developed length and interfacial density structure of the observed intrusions were found to correlate with an appropriately defined densimetric Froude number. The upstream intrusion that is produced by a constant flux of buoyant fluid discharged into a stream is one example of the phenomena identified as gravity currents. Simpson (1982) cited numerous examples of the formation of gravity currents in both natural and man-made flow situations.

Because of their widespread occurrence, gravity currents have been subjected to extensive study in recent years. The gravity currents examined in the present study are related to small-scale riverine, oceanic and limnological fronts, i.e. fronts that have lengthscales for which Coriolis forces are negligible. The term gravity current usually identifies all the fluid that makes up the buoyant layer. At the leading edge of the gravity current there is a density front where, within a relatively narrow region of horizontal extent, the density changes somewhat abruptly at the water surface. Surface convergence and concomitant downwelling occur at the leading edge of a surface front. In many cases there is a characteristic 'head' that is generally deeper than the following flow. However, in some cases, e.g. for gravity currents moving with the ambient current and for 'wedge' flows, the depth of the head can be less than the following flow. Although there is no universal shape to the front, it is distinguishable from the current that follows it.

The first prediction of the steady speed of propagation of the front of a gravity current moving along the bottom of an infinitely deep receiving basin of quiescent fluid was given by von Kármán (1940). Benjamin (1968) elucidated von Kármán's result and pointed out the importance of a breaking head-wave to produce the balance of forces necessary for steady propagation. They both showed that the front speed U is proportional to $(g'h)^{\frac{1}{2}}$, where g' is the reduced gravity and h is the depth of the following flow. The constant of proportionality for this case is $2^{\frac{1}{2}}$. Benjamin also showed the importance of fractional depth h/d on the frontal speed (where d is the depth of the channel). The densimetric Froude number $U/(g'h)^{\frac{1}{2}}$ decreases to about 1 for $h/d = \frac{1}{5}$ and to $2^{-\frac{1}{2}}$ for $h/d = \frac{1}{2}$.

For the case of a linearly stratified inflow into a homogeneous receiving water of infinite depth, Kao (1977) showed that the steady speed of the inflow front results in a densimetric Froude number equal to 1. Britter & Simpson (1978) examined an inviscid current model that included mixing in the frontal region. When there is mixing at the head and the fractional depth is small, Britter & Simpson found experimentally that the densimetric Froude number $U/(g'h)^{\frac{1}{2}}$ approaches $2^{\frac{1}{2}}$ as before; however, for this to be true, h must be taken as the densimetric mean level of the disturbed interface. This Froude number was found to vary with fractional depth and with the non-dimensional mixing rate $q = g'Q/U^3$, where Q is the volume flow rate of the dense source fluid per unit width of channel. Values of q are needed to complete the mathematical model and can either be measured experimentally or else deduced from the billow properties in the mixing region as described by Simpson (1982).

In other laboratory studies Simpson (1972, 1982) and Simpson & Britter (1979) examined the effects of boundary friction on the frontal motion of a bottom current. The main difference from the inviscid boundary model can be related to the height above the ground of the mean position of the foremost point of the head. For large values of Reynolds number, experimental observations suggest that this stagnation point is a constant distance above the bottom equal to about $\frac{1}{8}$ of the total head height.

By moving the floor adjacent to the current they concluded that the magnitude of the shear stresses along this boundary and its effects on the ambient flowfield control the substructure of the frontal zone and play a role in the size of the head.

Garvine (1981) derived jump conditions for the frontal zone of a shallow, buoyant surface layer. These jump conditions were proposed to facilitate the development of simplified hydrodynamic models of buoyant surface layers. Stigebrandt (1980) developed a hydraulic model to examine the dynamics of small-scale fronts. He examined the reduction of the frontal velocity caused by the secondary circulation induced by mixing in the frontal zone. Huppert (1982) and Didden & Maxworthy (1982) examined the frontal propagation of viscous gravity currents over rigid horizontal surfaces. Viscous gravity currents are unsteady phenomena, i.e. their fronts decelerate and their depths increase with time. They occur when the conditions of the flowfield are such that the dispersive action of the flow is relatively strong in comparison with the inertia of the induced motions and the gravitational forces produced by the density differences.

The detailed structure of the flowfield produced by a buoyant inflow into a quiescent receiving basin was examined numerically by Kao, Park & Pao (1978). Lin (1979) examined the same experimentally. They showed that the currents reach a steady speed of propagation and the layer behind the front appears to reach a steady, finite depth. The densimetric Froude number for the stratified gravity currents with finite fractional depths compared favourably with the inviscid model predictions of Benjamin (1968) and Kao (1977).

Cederwall (1971) presented experimental observations of wedge flows produced by a buoyant line source directed vertically into a stream. Heavy saline fluid was discharged downward into an open-channel flow. The jet descended to the bottom and upon impinging spread laterally. From a two-layer flow analysis Cederwall found that the mechanisms of upstream intrusion of jet effluent could be characterized by a source-densimetric Froude number based on the ambient flow velocity and the buoyancy flux from the source. Upstream intrusions were observed for source-densimetric Froude numbers less than experimentally determined critical values (critical values are of order 1 or less).

In the present study the mechanics of the gravity current produced by a constant-flux, buoyant discharge into a stream are examined. The simplest model of a stream into which a buoyant influx can be introduced is a two-dimensional open channel of infinite horizontal extent and finite depth. This model contains all the essential features of a stream necessary to examine the gravity currents produced by a buoyant effluent. If the effluent is introduced near the surface of the stream with zero horizontal momentum and relatively small vertical momentum (as compared with the buoyancy flux), the source fluid does not penetrate far from the surface of the stream, and it tends to spread horizontally almost instantaneously. If the stream flow is sufficiently weak and the flux of buoyancy sufficiently large, upstream intrusion is initiated. As the depth of the pool of buoyant fluid increases, the upstream intruding current rapidly approaches a quasi-steady maximum speed. Soon afterward, the front begins to decelerate as viscous friction takes over and the upstream intrusion approaches a state of zonal equilibrium. The deceleration towards equilibrium is not constant, nor is it monotonically increasing with time. Once the front begins to decelerate, gravity waves with frequencies related to the local Brunt–Väisälä frequency are excited on the downstream side of the front. As a quasi-steady state is reached, a two-zone equilibrium is established for the upstream intrusion. One of the zones is the frontal zone that propagates at a steady speed, albeit small, against

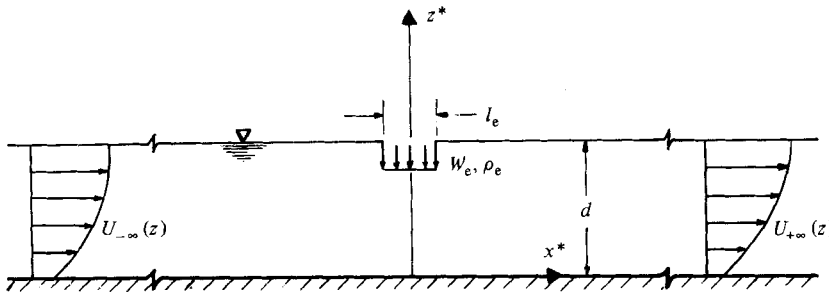

FIGURE 1. Sketch of the buoyant-inflow problem that includes the definition of the coordinate system.

the ambient current; consequently, it expands the current region behind it. In the current zone downstream of the frontal zone a steady state is approached with respect to the inertial frame of reference. In this zone a balance between the baroclinic production of vorticity and the vertical diffusion of vorticity is established. The present investigation indicates that the front of the upstream intrusion is not actually arrested. Rather, it moves very slowly against the ambient, streamwise current.

Although there is evidence that a totally arrested wedge is not possible, the intrusion tends toward such a state if the stream Froude number is sufficiently high. From a practical viewpoint, a totally arrested wedge and a very slow-moving wedge in equilibrium are essentially equivalent. On the other hand, as one might expect, for very weak streamwise current, the intrusion resembles an inflow into a quiescent receiving basin.

2. The flow problem

The flowfield produced by an instantaneously started buoyant source into a stream of infinite horizontal extent and finite depth is considered. Both the source fluid and the stream fluid are assumed miscible. Variations in the transverse direction as well as the effects of Earth rotation (Coriolis acceleration) are neglected. Because buoyancy is expected to play a dominant role in producing the predicted motions, the Boussinesq approximation is made, i.e. density variations are assumed to produce dynamically significant effects in the buoyancy term only. Mathematically, an initial-boundary-value problem is formulated and solved numerically for an incompressible, viscous, diffusive Boussinesq fluid undergoing laminar motions. The passive resistance to the motion attributable to viscous effects is explored by examining numerically two Reynolds numbers, viz 200 and 20. (From a practical point of view these Reynolds numbers may be interpreted as turbulent Reynolds numbers based on empirical turbulent viscosity coefficients. However, it is worth noting that this interpretation neglects the variation in turbulent transport coefficients produced by local density stratification.)

The initial-boundary-value problem considered here corresponds to starting a source of buoyant influx Q per unit width of channel with density ρ_e through a horizontal opening l_e centred at $x^* = 0$ into a stream moving at velocity U, with density ρ_0 and depth d. The source is located at the top of the channel, as illustrated in figure 1. The buoyant influx Q is equal to $W_e l_e$, where W_e is the average vertical velocity of the source fluid at $z^* = d$ and $-\frac{1}{2}l_e \leqslant x^* \leqslant \frac{1}{2}l_e$. We denote $\rho_e - \rho_0$ by $(\Delta\rho)_e$, the reference density deficit, and $(\rho - \rho_0)/\rho_0$ by γ, the density anomaly. Then $\gamma_e = (\rho_e - \rho_0)/\rho_0 = (\Delta\rho)_e/\rho_0$, and we define $g' = \gamma_e g$, where g is the acceleration due

to gravity. (When the inflow density difference is caused by a temperature difference with the ambient stream fluid, we may relate the density to the temperature by the approximate equation of state $\gamma = -\alpha(T - T_0)$, where α is the coefficient of thermal expansion.) We let D denote the diffusivity of the density anomaly (which may be taken as an eddy diffusivity in a crude model of turbulence) and let ν denote the kinematic viscosity (which may be taken as an eddy viscosity) and assume $D = \nu$ (i.e. we assume that $Sc = \nu/D = 1$).

Before we solve the coupled diffusion equation and the Navier–Stokes equations for a Boussinesq fluid, we will examine projected results by considering scaling arguments based on dimensional analysis and the known steady-state physics of the frontal motion of gravity currents. We introduce the timescale of the streamwise current, viz $\tau = d/U$, and the velocity scale associated with the influx of buoyancy, viz $U_d = (g'Q)^{\frac{1}{3}}$. Hence the following are the independent lengthscales of the problem: $L_0 = U_d d/U$, $h_0 = (Q^2/g')^{\frac{1}{3}}$, $h_\nu = (\nu d/U)^{\frac{1}{2}}$, l_e and d. By dividing the first four by the last, these scales combine to form four dimensionless parameters. They are

$$\frac{L_0}{d} = F_s^{-\frac{2}{3}}, \quad \frac{h_0}{d} = Q_s F_s^{\frac{2}{3}}, \quad \frac{h_\nu}{d} = Re^{-\frac{1}{2}}, \quad \frac{l_e}{d} = \frac{l_e}{d}, \tag{2.1}$$

where $Re = Ud/\nu$, $Q_s = Q/Ud$, $F_s = Q_s^{-\frac{1}{2}}|\gamma_e|^{-\frac{1}{2}}F$ and $F = U/(gd)^{\frac{1}{2}}$. (The source-densimetric Froude number F_s is the square root of the flux of inertia of the receiving stream divided by the flux of buoyancy discharged from the source, i.e. $F_s = [(Ud\rho_0 U^2/d)/(|\Delta\rho| g W_e l_e)]^{\frac{1}{2}}$. This indeed reduces to the previous formula.) What do the scales indicate about the flow problem?

If $F_s = 1$, then $L_0/d = 1$. Since U_d is a measure of speed of propagation of a density current discharged into a quiescent receiving basin, this implies that $U_d = U$. Thus for $F_s = 1$ the (inviscid) speed of propagation of a characteristic density current is equal to the streamwise current; consequently we would expect that $F_s > 1$ is a sufficient condition for no upstream intrusion. (It will be shown by numerical experiment that the critical source-densimetric Froude number is somewhat less than 1, depending upon the structure of the current.) At the condition $F_s = 1$, $h_0/d = Q_s$; i.e. the depth of the current is of the order of the volume flux of the source divided by the streamwise flux. The smaller F_s is, the shallower the surface layer; also, the smaller the value of F_s, the larger the upstream intrusion. Note that $(L_0/d)(h_0/d) = Q_s$ is a measure of the rate of volume displaced by the surface intrusion. For upstream intrusion to occur it is necessary that $F_s < 1.0$. For this case $L_0 > 1$, $L_0 \gg h_\nu$, and $h_0 \approx h_\nu$. In the present study l_e is such that the vertical input of momentum flux is small enough that the jet of buoyant fluid does not penetrate the depth of the developing surface layer. (In the numerical study the values of l_e/d ranged from 0.13 to 0.8.) In summary, we observe from the lengthscales characteristic of buoyant surface currents that a critical condition should exist for which upstream intrusion occurs, and it may be characterized by a source-densimetric Froude number F_s.

One of the major problems in examining layered flows and fronts produced by buoyant effluents discharged into streams is the definition of the interface between the two fluids. This is especially difficult if the fluids are miscible. Because of the diffusive nature of the flow, the constant-density surfaces are not necessarily parallel to the constant-stream-function surfaces, even in the steady state. The frontal region and surface layer described here are defined by the structure of the density-anomaly field. A criterion to determine the depth of the surface layer based on the numerical results is suggested and discussed later. It is based upon the balance of vorticity production in the upper layer once equilibrium is established.

A second problem in examining surface layers (or overflows) is that the prediction

of critical conditions is not expected to be universal. This is because the critical conditions depend on the structure of the current as it evolves. Recall that the characteristic speed of frontal propagation of a gravity current advancing in a quiescent receiving basin varies with depth of channel, density stratification of the current and boundary shear forces.

To examine further details of the genesis and evolution of an upstream intrusion, we must resort to the theoretical model of a viscous diffusive fluid described in §3.

3. Numerical solution

3.1. *Formulation*

The flow problem illustrated schematically in figure 1 will now be solved numerically by a finite-difference method. For convenience in developing the numerical procedure, the reference length and velocity were selected as d and U respectively. Thus the dimensionless coordinates are $(x, z) = (x^*/d, z^*/d)$, the dimensionless velocity components $(u, w) = (u^*/U, w^*/U)$ and the dimensionless time $t = t^*U/d$, where the asterisk denotes a dimensional quantity. With this scheme of dimensionless quantities, the equations that model the flow of a viscous, incompressible, Boussinesq fluid undergoing diffusive, two-dimensional, laminar motions in conservative form may be written as

$$\frac{\partial \gamma}{\partial t}+\frac{\partial (u\gamma)}{\partial x}+\frac{\partial (w\gamma)}{\partial z}=\frac{1}{Sc\,Re}\nabla^2\gamma, \tag{3.1}$$

$$\frac{\partial \zeta}{\partial t}+\frac{\partial (u\zeta)}{\partial x}+\frac{\partial (w\zeta)}{\partial z}=\frac{1}{F^2}\frac{\partial \gamma}{\partial x}+\frac{1}{Re}\nabla^2\zeta, \tag{3.2}$$

$$\nabla^2\psi=\zeta, \tag{3.3}$$

in which ζ, γ and ψ are the dimensionless vorticity, density difference and stream function, defined respectively by

$$\zeta=\frac{\partial u}{\partial z}-\frac{\partial w}{\partial x},\quad \gamma=\frac{\rho-\rho_0}{\rho_0},\quad u=\frac{\partial \psi}{\partial z},\quad w=-\frac{\partial \psi}{\partial x}.$$

The Laplacian is given by $\nabla^2=\partial^2/\partial x^2+\partial^2/\partial z^2$. The dimensionless parameters of the system are the Reynolds number Re, the Froude number F and Schmidt number Sc, where $Re=Ud/\nu$, $F=U/(gd)^{\frac{1}{2}}$ and $Sc=\nu/D$, in which ν is the kinematic viscosity, g is the gravitational acceleration and D is the diffusivity.

It should be noted that in this formulation the source-densimetric Froude number F_s does not appear explicitly as a parameter. However, F_s may be related to F, the inflow density anomaly γ_e and the volumetric flux ratio of the stream divided by the inflow by noting that $F_s=(Ud/l_e\,W_e)^{\frac{1}{2}}|\gamma_e|^{-\frac{1}{2}}Q_R^{\frac{3}{2}}F$, where Q_R is the volumetric flux of the streamflow upstream of the source.

Equations (3.1), (3.2) and (3.3) are solved numerically and are subject to boundary conditions representing the channel floor, upstream and downstream infinity, the free surface, and the initial condition representing the instantaneous start of a buoyant inflow. The upper boundary is assumed to be a free surface, and is represented by a horizontal plane at $z=1$. The rise in the free surface due to the intrusion of a lighter fluid into the ambient fluid is neglected because, as Kao *et al.* (1978) have demonstrated, for the density differences under consideration it is indeed negligible. In addition, since the channel is infinite in extent, there is no net rise of the free surface. On the free surface, i.e. the upper boundary, the shear stress is taken to be

zero; hence $\zeta = 0$. Also, on this boundary we allow heat to be transferred such that the amount of vertical heat transfer is proportional to the temperature difference between the surface temperature of the current and the ambient. The flux of heat through the lower boundary is taken to be zero (a constant-temperature boundary condition may be used instead). A solid boundary with either a no-slip or pure-slip condition is imposed at $z = 0$. The boundary conditions in terms of the dimensionless coordinate system may be summarized as follows:

(i) $$\psi = 0, \quad \frac{\partial \gamma}{\partial z} = 0, \quad \zeta = \frac{\partial^2 \psi}{\partial z^2} \quad (z = 0, \quad -\infty < x < +\infty),$$

(ii) $$\psi = \psi_B, \quad \frac{\partial \gamma}{\partial z} = \beta\gamma, \quad \zeta = 0 \quad (z = 1, \quad -\infty < x < -\tfrac{1}{2}l_e/d),$$

(iii) $$\psi = \psi_e(x), \quad \gamma = \gamma_e(x), \quad \zeta = 0 \quad (z = 1, \quad -\tfrac{1}{2}l_e/d < x < \tfrac{1}{2}l_e/d),$$

(iv) $$\psi = 1, \quad \frac{\partial \gamma}{\partial z} = \beta\gamma, \quad \zeta = 0 \quad (z = 1, \quad \tfrac{1}{2}l_e/d < x < +\infty),$$

(v) $$\psi = \psi_{+\infty}(z), \quad \gamma = 0, \quad \zeta = \zeta_{+\infty}(z) \quad (0 < z < 1, \quad x \to +\infty),$$

(vi) $$\psi = \psi_{-\infty}(z), \quad \gamma = 0, \quad \zeta = \zeta_{-\infty}(z) \quad (0 < z < 1, \quad x \to -\infty),$$

where β is a constant defined by $\beta = \kappa d/D$, with κ denoting an effective heat-exchange coefficient.

In addition to the boundary conditions for ψ, γ and ζ, the boundary conditions for u and w must be considered in order to compute the nonlinear terms in (3.1) and (3.2), in which u and w appear explicitly. These boundary conditions are: u (or $u = \partial\psi/\partial z$ if pure slip) and w vanish at $z = 0$; $u = 0$, $w = W_e/U$ at the inlet $z = 1$, $-\frac{1}{2}l_e/d < x < \frac{1}{2}l_e/d$; $u = U_{-\infty}(z)/U, w = 0$ as $x \to -\infty$; $u = U_{+\infty}(z)/U, w = 0$ as $x \to +\infty$. Note that U is taken to be the average horizontal velocity at $x \to +\infty$. The horizontal velocity component at $z = 1$ excluding the source can be computed from the defining relations $u = \partial\psi/\partial z$. Also, at $z = 0$ the vertical component of velocity $w = -\partial\psi/\partial x = 0$.

The initial condition for a sudden start of an inflow at the opening is a potential flow with ψ satisfying the homogeneous equation $\nabla^2\psi = 0$ and with $\gamma = 0$ everywhere. For a source at $z = 1$, $x = 0$ in a uniform stream between frictionless walls at $z = 0$ and $z = 1$, it can be shown that the stream function is given by the formula

$$\psi = (1 - Q_s)\, z + \frac{Q_s}{\pi}\left(\tfrac{1}{2}\pi z + \tan^{-1}\left(\tanh \tfrac{1}{2}\pi x \tan \tfrac{1}{2}\pi z\right)\right). \tag{3.4}$$

Equation (3.4) is for a point source of strength Q_s at $x = 0$, $z = 1$ and uniform flow at $x \to +\infty$ between the walls $z = 0$ and $z = 1$. The Laplace equation for a source of finite width can be solved by numerically integrating $\nabla^2\psi = 0$ between $z = 0$ and $z = 1$ and $-\infty < x < +\infty$ with a finite-width source at $z = 1$ between $-\frac{1}{2}l_e/d < x < \frac{1}{2}l_e/d$. One method is over-relaxation, which is a numerical-analysis procedure for elliptic equations. Equation (3.4) provides the necessary guess for the potential-flow initial condition sought. If an initial condition for a point source in a shear flow is sought, then the first term on the right-hand side of (3.4), viz $(1 - Q_s)\, z$, may be replaced by

$$(1 - Q_s)\{a_1 z + a_2 z^2 + a_3 z^3\}, \tag{3.5}$$

where, for a uniform flow as $x \to -\infty$, $a_1 = 1$, $a_2 = a_3 = 0$; for a linear shear flow (Couette flow) as $x \to -\infty$, $a_2 = 1$, $a_1 = a_2 = 0$; and for a parabolic profile (Poiseuille

flow) as $x \to -\infty$, $a_1 = 0$, $a_2 = +\frac{3}{2}$, $a_3 = -\frac{1}{2}$. The initial vorticity distribution is zero for the first case, constant for the second and equal to $\partial^2/\partial z^2$ of (3.5) for the third. It is assumed that the source flow is initially irrotational.

When the density change is due to temperature difference in the surface current, changes in surface tension due to horizontal temperature variation at the free surface induce a shear stress at the free surface. As pointed out by Kao *et al.* (1978), it can be shown that for the temperatures considered in the present investigation the effect of free-surface curvature is negligible.

3.2. *Stretched coordinate system*

The horizontal scale in the present problem extends from minus infinity to plus infinity. A dilemma is posed by conflicting requirements: keeping the finite-difference grid mesh fine in the vicinity of the source, where the gradients are largest; and, at the same time, having the outer grid points far enough away from the source for them to approximate closely the infinities. Because the outer boundaries are not actually at infinity, they require special treatment to prevent the inevitable partial reflection whenever the fastest-propagating disturbances reach them. One approach to alleviating the problem of the infinite domain is to transform the infinite domain into a finite domain; thence the boundary conditions at infinity can be handled directly. In addition the resolution in the vicinity of the source is increased. This method of improving accuracy while maintaining numerical stability is applied herein. The objective is to maintain equal grid spacings, which are more desirable than unequal grid spacings from the viewpoint of numerical accuracy (see Roache 1972). A similar method was applied by Pao & Kao (1974).

We seek a coordinate system $(\bar{x}, \bar{z})$ whose mapping to ordinary Cartesian coordinates (x, z) is such that $\bar{x}$ varies from -1 to $+1$ as x varies from $-\infty$ to $+\infty$, and $\bar{z}$ varies from 0 to $+1$ as z varies from 0 to $+1$. The reason for transformation of the vertical (z) coordinate is so that it has the property of increasing the resolution of the flow-field in the vicinity of the free surface. This property is desired because the source of thermal discharge is located at the free surface, and it is expected that the discharged fluid will float in the vicinity of the free surface as it propagates from the source. The transformations for such a system are given by

$$\bar{x} = \tanh ax, \tag{3.6}$$

$$\bar{z} = \frac{\sinh bz}{\sinh b}, \tag{3.7}$$

where a and b are scale factors corresponding to the horizontal and vertical coordinate transformations respectively. Upon substituting the transformation relations (3.6) and (3.7) into the equations of motion (3.1)–(3.3), we obtain

$$\frac{\partial \gamma}{\partial t} + p_1 q_1 \left\{\frac{\partial (u_1 \gamma)}{\partial \bar{x}} + \frac{\partial (w_1 \gamma)}{\partial \bar{z}}\right\} = \frac{1}{Sc\,Re}\left\{p_1^2 \frac{\partial^2 \gamma}{\partial \bar{x}^2} + q_1^2 \frac{\partial^2 \gamma}{\partial \bar{z}^2} + p_2 \frac{\partial \gamma}{\partial \bar{x}} + q_2 \frac{\partial \gamma}{\partial \bar{z}}\right\}, \tag{3.8}$$

$$\frac{\partial \zeta}{\partial t} + p_1 q_1 \left\{\frac{\partial (u_1 \zeta)}{\partial \bar{x}} + \frac{\partial (w_1 \zeta)}{\partial \bar{z}}\right\} = \frac{p_1}{F^2}\frac{\partial \gamma}{\partial \bar{x}} + \frac{1}{Re}\left\{p_1^2 \frac{\partial^2 \zeta}{\partial \bar{x}^2} + q_1^2 \frac{\partial^2 \zeta}{\partial \bar{z}^2} + p_2 \frac{\partial \zeta}{\partial \bar{x}} + q_2 \frac{\partial \zeta}{\partial \bar{z}}\right\}, \tag{3.9}$$

$$p_1^2 \frac{\partial^2 \psi}{\partial \bar{x}^2} + q_1^2 \frac{\partial^2 \psi}{\partial \bar{z}^2} + p_2 \frac{\partial \psi}{\partial \bar{x}} + q_2 \frac{\partial \psi}{\partial \bar{z}} = \zeta, \tag{3.10}$$

where

$$u_1 = \frac{\partial \psi}{\partial \bar{z}}, \quad w_1 = -\frac{\partial \psi}{\partial \bar{x}},$$

$$p_1 = a(1-\bar{x}^2), \quad p_2 = -2a\bar{x}p_1,$$

$$q_1 = \frac{b}{\sinh b}\{1+[\bar{z}\sinh b]^2\}^{\frac{1}{2}}, \quad q_2 = b^2\bar{z}.$$

If $p_1 = q_1 = 1$ and $p_2 = q_2 = 0$ then the coordinate system becomes the unstretched system.

3.3. *Numerical-analysis scheme*

The numerical integration method applied to investigate the problem of a thermal inflow into the current of a stream is an explicit finite-difference method that possesses both the transportive and conservative properties described in detail by Roache (1972). Central differences in space and forward differences in time are used, except for the nonlinear terms in the equations of motion, for which a special three-point non-central differencing method is adopted. The latter is analogous to the method described and applied by Torrance & Rockett (1969) and Pao & Kao (1974). Equations (3.8) and (3.9) are parabolic, while (3.10) is elliptic. Therefore (3.10) is solved by a standard over-relaxation technique. This scheme has been successfully applied by Pao & Kao (1974) and Kao *et al.* (1978) in studies of similar problems (for details of applying this scheme see Pao & Kao 1974). The scheme is explicit; therefore, in comparison with some implicit schemes, smaller time steps are required. However, it is the evolution of the flow and not the large-time solutions that is of interest here. This finite-difference scheme retains something of the second-order accuracy of centred space derivatives. The stability of the scheme is gained from the non-centred space derivatives for the nonlinear advective terms that result in computational damping (see Torrance 1968).

This damping acts very much like a diffusive effect. The vorticity is known to be most sensitive to numerical error; see Lugt & Haussling (1974). Therefore, in the present study the truncation errors, i.e. the terms that cause the false diffusion, in the solution of the vorticity equation were examined in order to establish the numerical accuracy of the computational results. A computer code was written to calculate the false diffusion throughout the domain of interest. The false diffusion was compared with the advective term and the physical diffusion term at all the grid points. The results of the comparison confirmed the results presented by Kao *et al.* (1978). Therefore the false diffusion (as expected) did not mask the physics of the problem. Indeed, a comparison of results obtained with a higher-order scheme (which does not contain the large false diffusion formally found in the finite-difference scheme described above) confirmed this. In fact, it is concluded that, since two different numerical schemes led to the same results, the numerical-analysis method selected is correct, and the false diffusion does not mask the physics.

The higher-order scheme was based on central differences in space and the DuFort–Frankel molecule (as used by Lugt & Haussling 1974). It was abandoned in favour of the upwind scheme for two reasons: (1) it has an error in diffusion that propagates against the current which is not in the upwind scheme; for a derivation of this problem see Roache (1972); (2) the upwind scheme has been successfully applied by Kao *et al.* in examining the physical properties of similar flowfields. Since

Case	γ_e	Sc	Re	F	F'	Q_s	Q_R	l_e/d	F_s^2	β
1	−0.003	1	1000	0.003	0.055	0.5	0.5	0.13	0.0007	5
2	−0.003	1	200	0.009	0.131	0.2	0.8	0.267	0.0691	0
3	−0.009	1	200	0.009	0.076	0.2	0.8	0.267	0.0230	0
4	−0.012	1	200	0.009	0.66	0.2	0.8	0.267	0.0173	0
5	−0.005	1	200	0.030	0.33	0.23	0.77	0.4	0.357	0
6	−0.003	1	200	0.009	0.131	0.2	0.8	0.267	0.599	0
7	−0.003	1	200	0.009	0.131	0.2	0.8	0.267	0.768	0
8	−0.0025	1	200	0.025	0.5	0.25	1.0	0.4	1.0	5
9	−0.012	1	20	0.009	0.066	0.2	0.8	0.8	0.0173	0
10	−0.012	1	20	0.012	0.088	0.2	0.8	0.8	0.0307	0

TABLE 1. List of overflow cases computed

we are interested in the inception of upstream intrusion, the first reason cited dictates the use of the upwind scheme.

The finite-difference mesh selected consisted of 61 grid points in the horizontal direction and 41 grid points in the vertical direction. The algorithm or numerical procedure adopted in this investigation was described by Kao *et al.* (1978). A computer program was written in Fortran for batch execution and has been implemented on a CDC-6000 series computer with a central memory requirement of approximately 170K (Octal) of 60 bit words. This word length tends to minimize round-off errors. In most cases the time increment was set to be 2.0×10^{-3}. Some of the figures were created by using an off-line Calcomp plotter. A special computer program was prepared to do the plotting. Needless to say, this plotting procedure turned out to be invaluable in the data reduction and for the evaluation of the results.

4. Results and discussion

The surface currents produced by a buoyant effluent discharged into a stream that were examined in the present study cover a range of inflow (or source) densimetric Froude number F_s that extends from 0.026 to 1.0. The cases computed are summarized in table 1. In all cases the velocity distribution at the mouth of the discharge is uniform and vertically downward into the stream; therefore, its initial horizontal momentum is zero. The discharge opening is relatively wide (l_e/d varies from 0.13 to 0.8); hence the vertical velocity is small enough so that the jet does not penetrate far from the free surface. At time zero the density deficiency of the source is turned on instantaneously. The upper and lower boundaries of the stream are pure-slip except for case 10. Therefore the upstream and downstream velocity profiles are initially uniform. In case 10 a no-slip condition was imposed along the lower boundary; also, the streamwise velocity profile was assumed to be fully developed and parabolic at time zero.

This study determined what is the critical condition for the occurrence of an upstream intrusion and what are the various stages in the development process when it occurs. Case 1 was computed to examine the principal features of a buoyant surface current (or overflow) at small F_s. The upstream intrusion for this case is similar to the surface currents produced by a buoyant discharge into a quiescent receiving basin. Cases 2–5 were computed to examine the conditions required for the occurrence of an upstream intrusion. In addition, cases 6–8 were computed to examine the critical

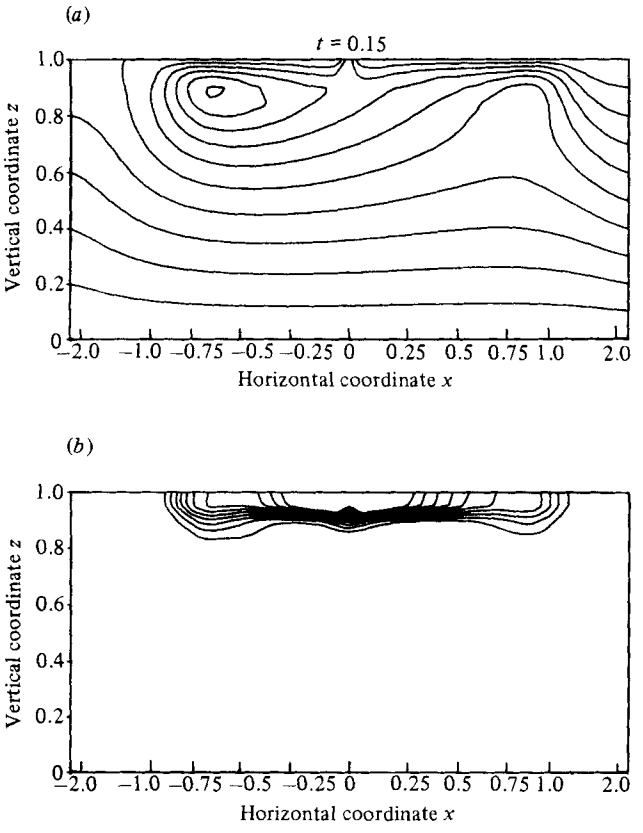

FIGURE 2. Streamlines (*a*) and isopycnics (*b*) of an overflow in a uniform, homogeneous current at $t = 0.15$; $Q_s = 0.5$, $F_s = 0.026$. Each isopycnic represents successive decreases in γ of $0.1\gamma_e$ from the source value of γ_e.

value of the inflow densimetric Froude number by comparing the surface layers produced by inflows near critical densimetric conditions ($0.5 < F_s^2 < 1.0$). A critical value of inflow densimetric Froude number is identified. Cases 4, 9 and 10 were computed to examine the various stages in the development process of the upstream intrusion. The evolution from inception to a state of zonal equilibrium is described for $F_s < 0.5$. Four stages in the development process are identified. The intrusion starts as an inviscid gravity current with a propagation speed greater than the surface velocity of the stream. The front accelerates to a plateau speed. Subsequently, the current decelerates towards a two-zone equilibrium. The first zone is the frontal zone, in which the front approaches a steady speed of advance, albeit small. The second zone is the zone encompassing the surface current following the frontal zone, in which steady state is approached with respect to the inertial frame of reference. Thus the frontal zone moves upstream expanding the following-current zone. In all cases, the leading edge of the density front is adequately defined by the $\gamma = 0.1\gamma_e$ isopycnic because it is near this isopycnic that surface convergence with concomitant downwelling occurs. However, it was found that this isopycnic does not necessarily define the interface between the following current and the stream fluid. Therefore a criterion for the location of the interface between the surface current of the diluted effluent and the lower layer of stream fluid in the two-layered following-current zone was developed.

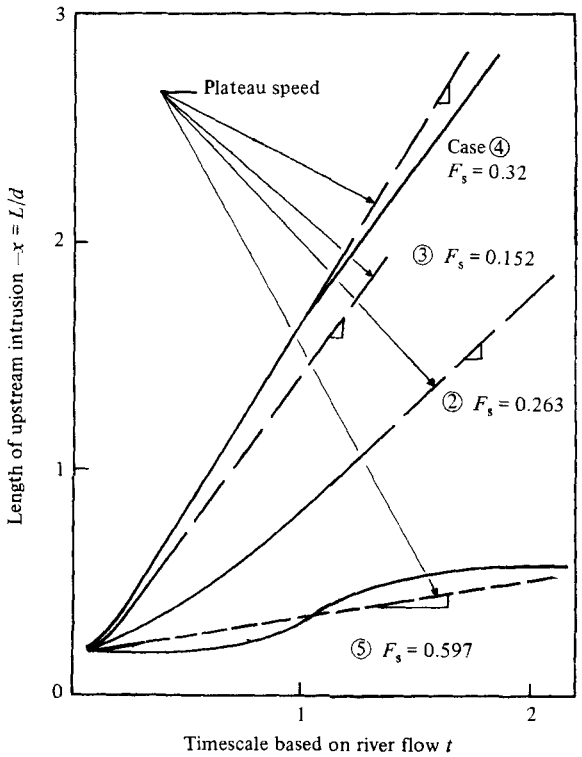

FIGURE 3. Horizontal length of several upstream intrusions versus time. This figure illustrates the effect of source-densimetric Froude number F_s on the predicted plateau speed.

The streamline pattern of case 1 at time $t = 0.15$ is presented in figure 2(*a*) to illustrate that once the buoyant fluid enters the stream its tendency is to spread horizontally and almost immediately (within a few seconds†) with a dramatic altering of the streamlines from the initial pattern of a source flow in a channel flow. The inflow densimetric Froude number for this case is 0.026. The corresponding isopycnic contours are illustrated in figure 2(*b*). For this time step the buoyant effluent has moved against the streamwise current about 1.0*d* from the source. The depth of the parent pool (i.e. the surface layer below the source location) is approximately 0.12*d*. The frontal region exhibits the characteristic features of buoyant overflows, including the characteristic head shape and the outcropping of the isopycnics. Because the inflow-layer densimetric Froude number is quite small, the developing surface layer (or overflow) is relatively shallow and spreads horizontally such that the upstream intrusion at this stage is propagating like an inviscid gravity current. In fact, in a reference frame moving with the upstream front, the upstream gravity current has a densimetric Froude number equal to approximately 1.0; this is expected based on the measurements and predictions of similar surface currents reported by Kao *et al.* (1978), and measurements reported by Keulegan (1958).

† The characteristic parameters of rivers with relatively weak current in which upstream intrusions of buoyant effluents have been observed are as follows (see e.g. Polk *et al.* 1971). Rivers of this type have Froude numbers of order 0.01. If, for example, the depth of the river is 12 m, then the average river velocity for a constant-width channel is approximately equal to 11 cm/s. Thus the characteristic timescale for this river is about 2 min.

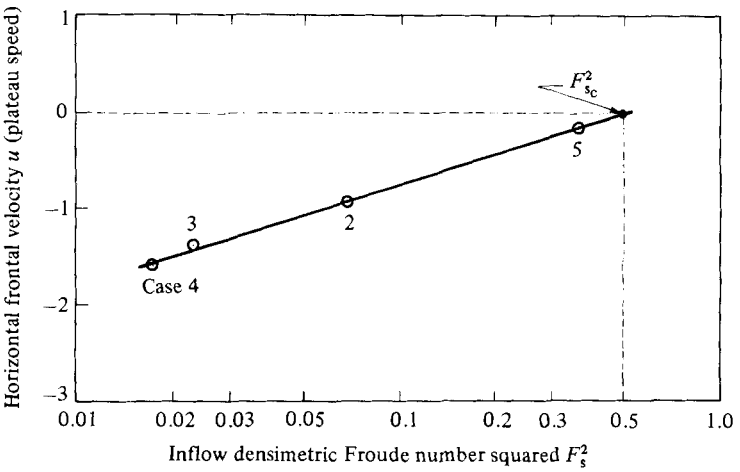

FIGURE 4. Surface speed (i.e. the plateau speed) of the upstream front as a function of $\ln F_s^2$ corresponding to the cases in figure 3. This plot illustrates the predicted, extrapolated critical value.

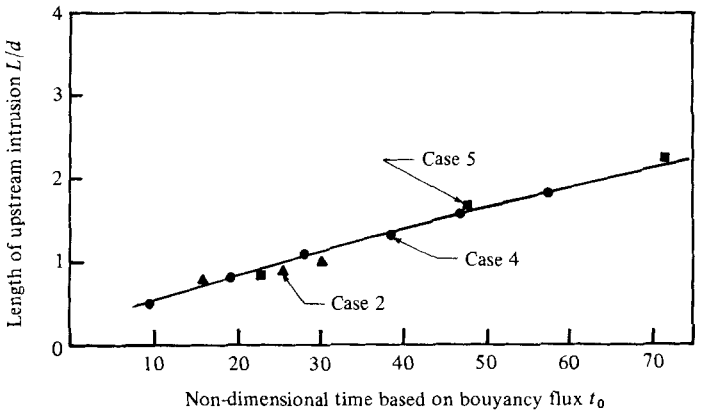

FIGURE 5. Correlation of the length of the upstream intrusion versus a buoyancy timescale based on the inviscid propagation speed of a gravity current for three values of source-densimetric Froude numbers represented by cases 2, 4 and 5.

4.1. *Critical condition of upstream intrusion*

If upstream intrusion occurs there are four successive stages of development. They are: initial acceleration, peak (or plateau) speed, deceleration and equilibrium. The first two stages govern the initiation process; thus, they are considered next. Cases 2–4 are all for $F_s < 0.5$. The difference between cases 2, 3 and 4 is the density anomaly of the source. Case 5 is a case where $F_s = 0.597$. For these cases the length of intrusion for time steps up to $t = 2.0$ and the corresponding plateau speeds attained are compared in figures 3 and 4 respectively. Extrapolating the curve in figure 4 to $U_d^{up} = 0$, we obtain an extrapolated critical value of F_s equal to 0.71. This critical case was computed; however, although the upstream frontal speed was less than that for case 5, the front still intruded upstream. Therefore the short-time solutions of additional cases with $0.7 < F_s < 1.0$ were computed to predict more precisely the critical value of F_s. The critical value was then determined to be 0.85. Cederwall (1971) determined experimentally that the critical value of the source-densimetric Froude

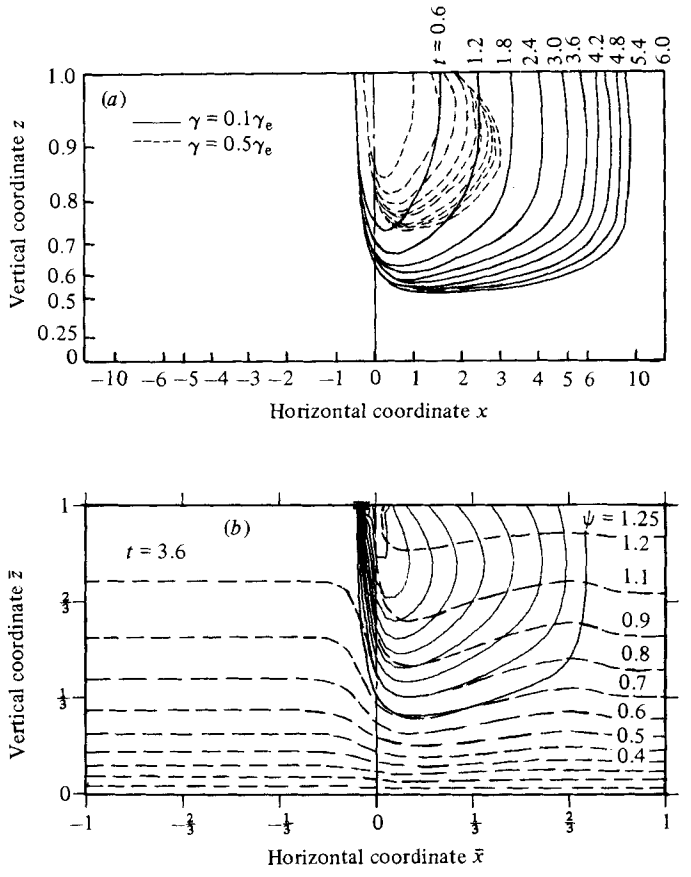

FIGURE 6. (*a*) Location of the frontal interface ($\gamma = 0.1\gamma_e$) and the $\gamma = 0.5\gamma_e$ isopycnic for several time steps for a source-densimetric Froude number slightly greater than critical; $F_s = 1.0$, $Q_s = 0.25$, $Re = 200$. (*b*) Streamlines and isopycnics for this case at $t = 3.6$. Each isopycnic represents successive decreases in γ of $0.1\gamma_e$ from the source value γ_e.

number F_s was of order 1 or less. There was a slight dependence on the parameter $l_e/Q_s^2 d$; the small values of $l_e/Q_s^2 d$ gave slightly smaller critical Froude numbers. The values of $l_e/Q_s^2 d$ for the cases examined here are all equal to about 0.7. For $l_s/Q_s^2 d$ equal to 0.7, Cederwall observed a critical value of order 0.8. Thus his experiments provide qualitative confirmation of the predicted critical value.

The upstream fronts for cases near critical ($F_s < F_{sc}$) take a relatively long time to reach the deceleration stage. The computed solutions for case 5 show that at time step $t = 11.2$ (or approximately 22 min from startup) the upstream front has not yet begun to decelerate. In contrast, the frontal motion of case 4 ($F_s \ll F_{sc}$) commences to decelerate at $t = 1$ (or approximately 2 min from startup). The predicted results of case 5 are characteristic of cases for which the buoyant overflow is near critical. The plateau speed for this case is taken to be the average of the upstream frontal advance speed. A principal feature of case 5 and one strikingly different from cases 2–4 (cf. figure 3) is that the upstream frontal motion is oscillatory from the time the buoyant source is turned on.

The initiation process may be characterized by the inviscid propagation of a gravity-motivated current. If we renormalize the time by multiplying the timescale

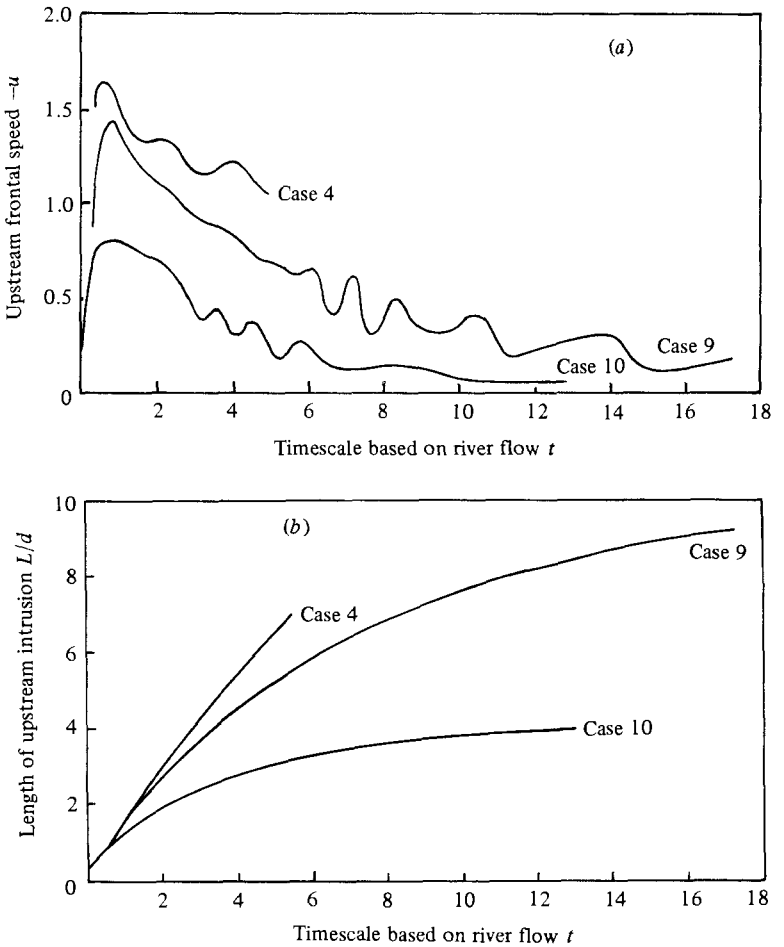

FIGURE 7. (*a*) Propagation speed of the upstream front ($\gamma = 0.1\gamma_e$ at $z = 1$) versus time for cases 4 ($F_s = 0.132$, $Re = 200$), 9 ($F_s = 0.132$, $Re = 20$) and 10 ($F_s = 0.195$, $Re = 20$). (*b*) Corresponding lengths of upstream intrusion as a function of time.

in terms of the river scale by $(h_0/U_d)/(d/U) = (Q_s F'^4)^{\frac{1}{3}}$, we obtain a new timescale associated with the influx of buoyancy. This was done for cases 2, 4 and 5. The length of the upstream intrusions versus this new timescale collapse to one line (see figure 5). Thus the front starts as an inviscid gravity current.

The numerical solutions for case 8 are summarized in figure 6. The source-densimetric Froude number for this case is exactly equal to unity. We see that in this case no upstream intrusion is present. The frontal interface as indicated by the $\gamma = 0.1\gamma_e$ line at successive times is shown in figure 6(*a*). It is seen that the upstream interface assumes a perfectly stationary position. Figure 6(*b*) shows the streamline and isopycnic patterns at a fixed time. This case represents an F_s slightly greater than that of the critical case of no upstream intrusion.

4.2. *Development process of upstream intrusion*

The development process or evolution of an upstream intrusion from the initiation stage to the stage of zonal equilibrium is determined by examining the solutions of

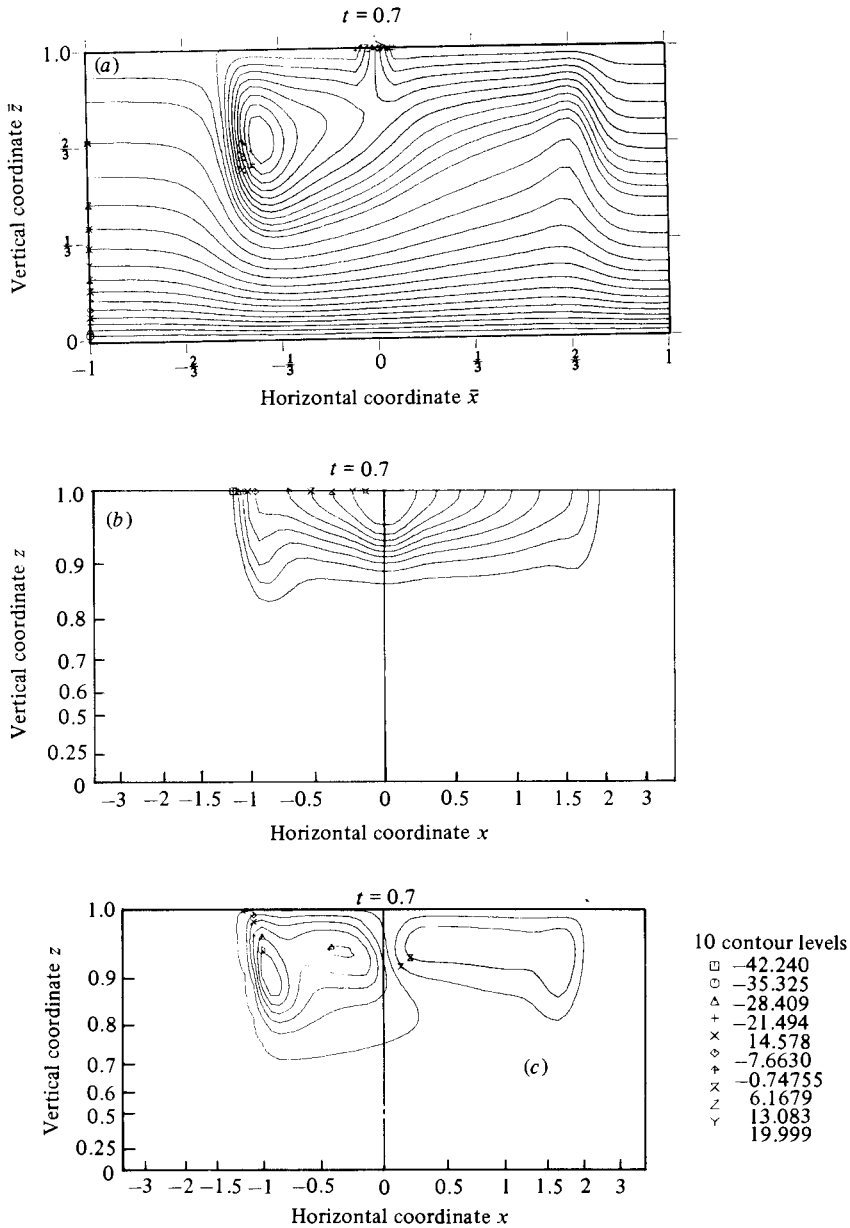

FIGURE 8. Streamlines (*a*), isopycnics (*b*) and isolines of the *y*-component of vorticity (*c*) for an overflow, case 4, at $t = 0.7$; $F_s = 0.132$; $Re = 200$; $Q_s = 0.2$. Each isopycnic represents a successive decrease in γ of $0.1\gamma_e$ from the source value γ_e.

three cases, viz 4, 9 and 10. The speeds of propagation of the upstream fronts for the three cases are compared in figure 7 (*a*). Their distances from the source point as a function of time are compared in figure 7 (*b*). Initial acceleration occurs when the characteristic speed of frontal propagation is greater than the local stream speed. Because of the resolution of the timescale plotted in figure 7 (*a*), the plateau speed appears as a peak in the velocity. In the deceleration stage the frontal motion is oscillatory with frequencies characteristic of internal waves, i.e. for cases 9 and 10

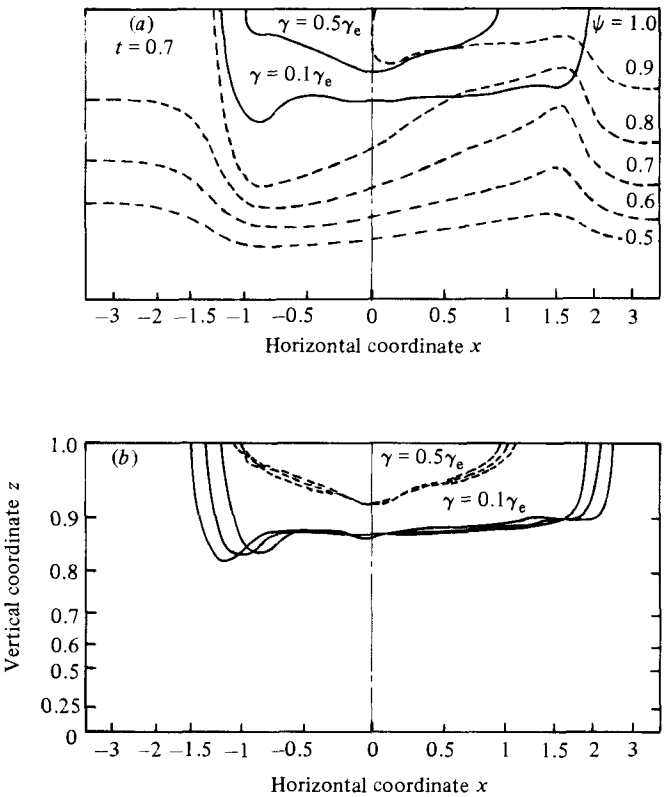

FIGURE 9. (*a*) Comparison of streamline patterns and two isopycnics ($\gamma = 0.1\gamma_e$ and $0.5\gamma_e$) at time $t = 0.7$ for case 4 ($F_s = 0.132$, $Q_s = 0.2$, $Re = 200$). (*b*) Comparison of the isopycnic representing the frontal interface ($\gamma = 0.1\gamma_e$) and the $\gamma = 0.5\gamma_e$ isopycnic for time steps $t = 0.7$, 0.8 and 0.9.

the variations in the Brunt–Väisälä cut-off frequency that characterizes internal wave motion were computed in the frontal region and found to be representative of the frequencies observed. Note that the frequencies of the oscillation decrease with time and the amplitude appears to be damped as the front approaches an equilibrium speed.

The length of the intrusion decreases with increase in Froude number; its length depends upon the streamwise inertial flux as compared with the gravity-imposed pressure field caused by the buoyancy flux of the source. The length also decreases with Reynolds number since an increase in viscous dissipation reduces the kinetic energy of the intrusion. The theoretical predictions indicate that the frontal region is not actually arrested; instead, as the streamwise Reynolds number decreases and/or the Froude number increases the terminal speed of frontal propagation is decreased.

The streamlines, isopycnics and isolines of the y-component of vorticity for time $t = 0.7$ of case 4 are presented in figure 8. Although the source-densimetric Froude number for this case is a factor of five greater than that for case 1, the depth of the surface layer is about the same in both cases, i.e. it is about $0.12d$ (cf. figure 2*b*). Significant increases in the buoyant-surface-layer depth as delineated by the $\gamma = 0.1\gamma_e$ isopycnic (at a location just below the source, i.e. at $x = 0$) begin to occur for F_s greater than approximately 0.2. (This was determined by comparing the

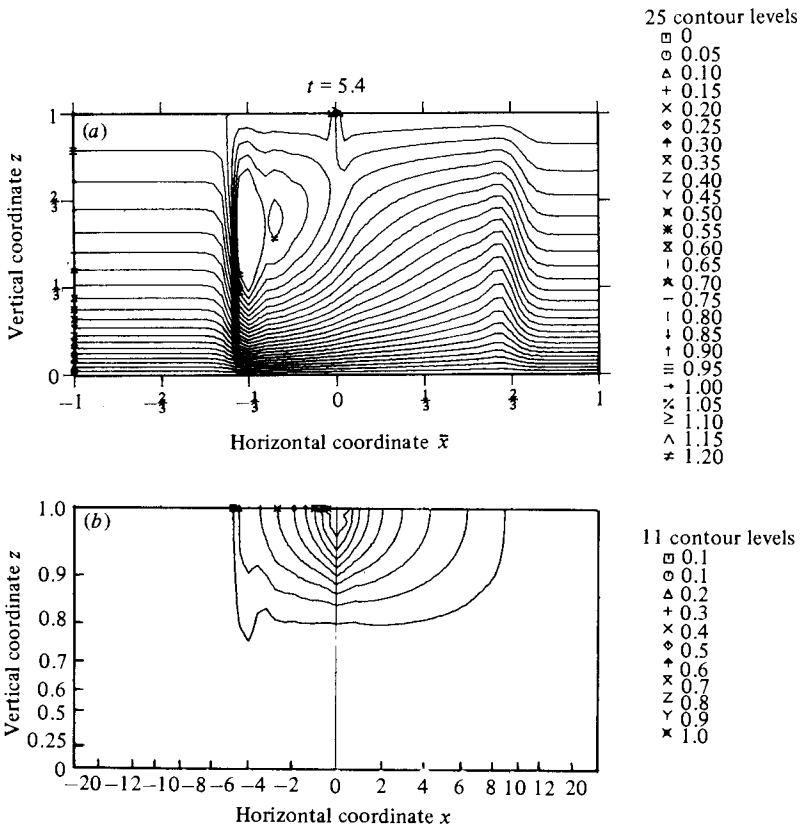

FIGURE 10. Streamlines (*a*) and isopycnics (*b*) for case 4 ($F_s = 0.132$, $Q_s = 0.2$, $Re = 200$) at time $t = 5.4$. This plot illustrates the circulatory flow developing in the surface layer following the upstream front.

position of the $\gamma = 0.1\gamma_e$ isopycnics for cases 2–4 during their initial stages of development, i.e. for $t < 2$.) The qualitative structure of the isopycnic contours for cases 2–4 is the same as the structure already described for case 1. The distinctly deeper frontal zone (or 'head') depicted by the shape of the $\gamma = 0.1\gamma_e$ isopycnic is characteristic of the small source-densimetric Froude-number cases (i.e. $F_s < 0.5$).

Figure 9(*a*) illustrates the relationship between the $\gamma = 0.1\gamma_e$ isopycnic and the streamline pattern at time $t = 0.7$ for case 4. For this case the $\gamma = 0.1\gamma_e$ isopycnic appears to model the interface of the frontal region adequately. The surface convergence and downwelling are shown to occur about the frontal boundary, defined by $\gamma = 0.1\gamma_e$. Figure 9(*b*) illustrates the relationship between the intermediate isopycnic ($\gamma = 0.5\gamma_e$) and the isopycnic representing the front of the overflow (viz $\gamma = 0.1\gamma_e$) for three time steps. Note that the upstream advance of $\gamma = 0.1\gamma_e$ is not the same as the advance of $\gamma = 0.5\gamma_e$. As the flowfield evolves, a secondary rotor is produced in the surface layer behind the upstream front. At time step $t = 0.7$ a secondary rotor appears to be starting; this is indicated by the isolines of the y-component of vorticity presented in figure 8(*c*). In order to examine long-time solutions a coarser mesh was required. The mesh size was altered and long-time solutions were computed. A secondary rotor indeed occurs at time steps greater than 0.7, as illustrated in figure 10 for time $t = 5.4$. Head waves can be observed at the

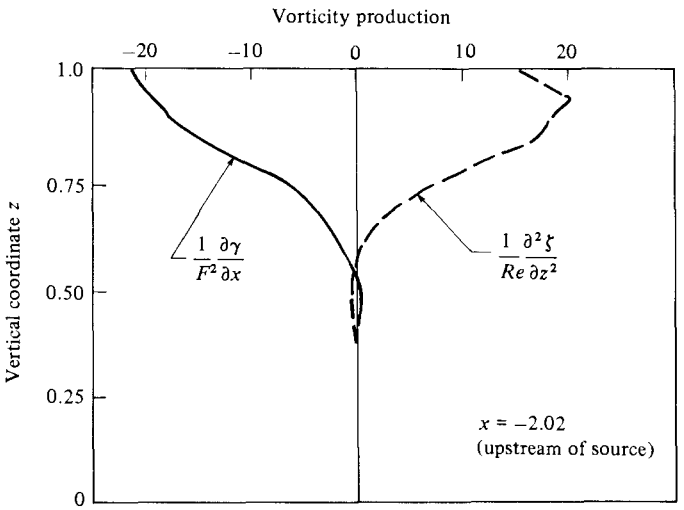

FIGURE 11. Balance of vorticity production in current following the upstream front at $x = -2.02$ upstream of the source for the overflow case 4 ($F_s = 0.132$, $Q_s = 0.2$, $Re = 200$).

leading edge of the frontal zones; as expected, the downstream disturbance is the weaker one (because the surface layer and stream are coflowing downstream and counterflowing upstream).

The flowfield between the frontal zones approaches steady state in the inertial frame of reference sooner than in the frontal regions. Eventually, the upstream frontal motion settles down to a nearly constant speed of advance. In fact, for $t = 5.0$ the balance of vorticity production at a distance $x = -2.02$ from the source is a balance between the production of vorticity caused by buoyancy and the diffusion of vorticity, i.e.

$$-\frac{1}{F^2}\frac{\partial \gamma}{\partial x} = \frac{1}{Re}\frac{\partial^2 \zeta}{\partial z^2} \tag{4.1}$$

in this region (see figure 11). Therefore, in the two-layered stratified flow following the upstream front, the dynamics of the upper layer is decidedly linear. The streamlines and isopycnics are not parallel to the horizontal coordinate and the horizontal velocities are not constant with the x-coordinate. This is in contrast with the overflow into a quiescent receiving basin for which Kao *et al.* (1978) predicted a constant-depth layer following the frontal zone. Longer-time solutions for this case were abandoned because, as indicated in figure 7, very large times (and excessively long computer time) would be required to approach equilibrium. Therefore the next step was to increase diffusion by decreasing the Reynolds number from 200 to 20.

Case 9 is the same as 4 except for the order-of-magnitude change in diffusion. As expected, the deceleration is substantially decreased for the lower-Reynolds-number case (see figure 7). The dissipative mechanism of internal friction causes a dramatic reduction in upstream propagation of the front.

Garvine (1974) described a part of the dissipative mechanism that may also work to oppose the propagation of a density front. It is associated with the volume flux entrained across the interface between the surface layer and the ambient receiving water. Negative values of volume flux within the upstream surface current behind the front correspond to downward entrainment, i.e. entrainment of lighter surface

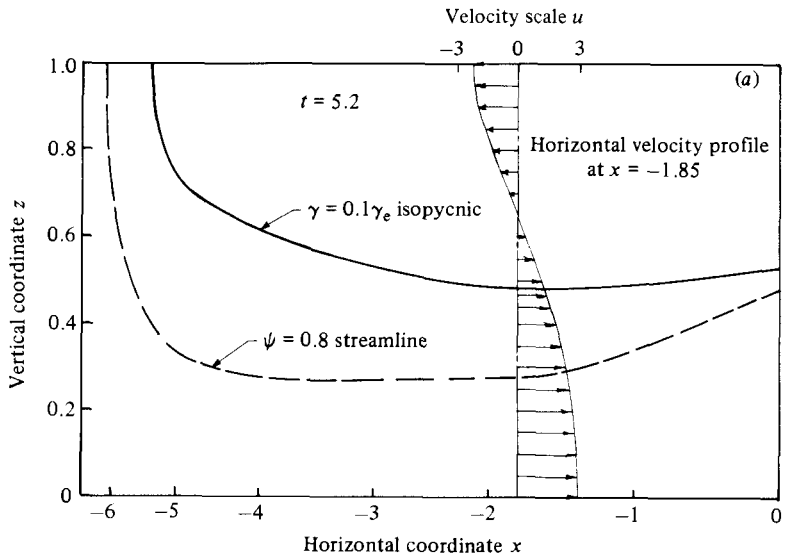

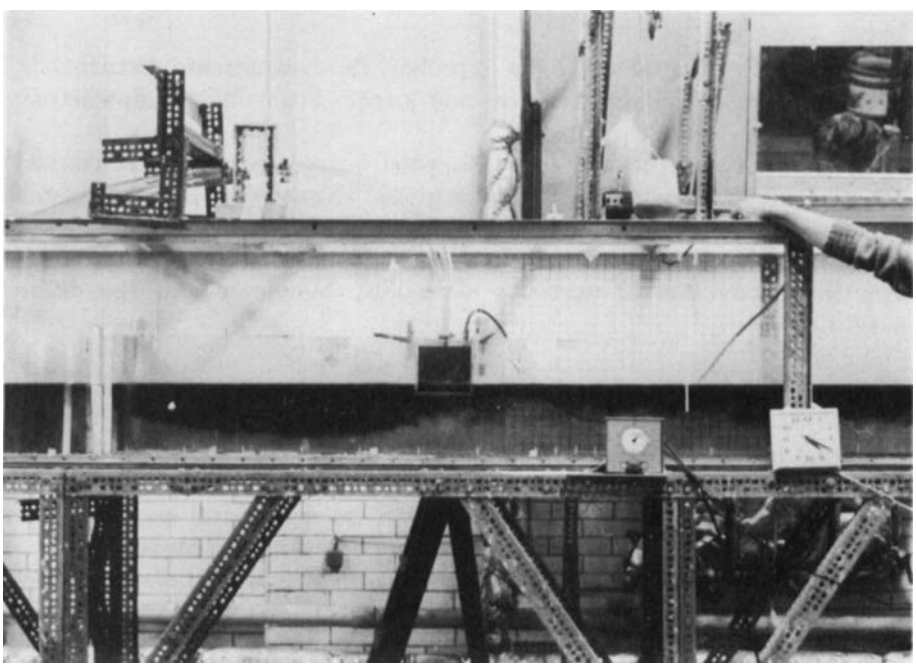

FIGURE 12. (*a*) Comparison of the dividing streamline ($\psi = 0.8$) and the $\gamma = 0.1\gamma_e$ isopycnic for $t = 5.2$ for case 9 ($F_s = 0.132$, $Re = 20$, $Q_s = 0.2$). (*b*) Photographs of a laboratory-produced upstream intrusion ($F_s^2 \approx 0.02$).

fluid into the heavier bottom fluid. For this direction of entrainment Garvine (1974) showed that more friction is required to slow the frontal system to a steady state. He also pointed out that better correlation with the field data of oceanic fronts was obtained when downward entrainment was assumed. In the present investigation figure 12 (*a*) illustrates the predicted downward entrainment for the two-layer system of case 9. The direction of entrainment is easily verified by comparing the location

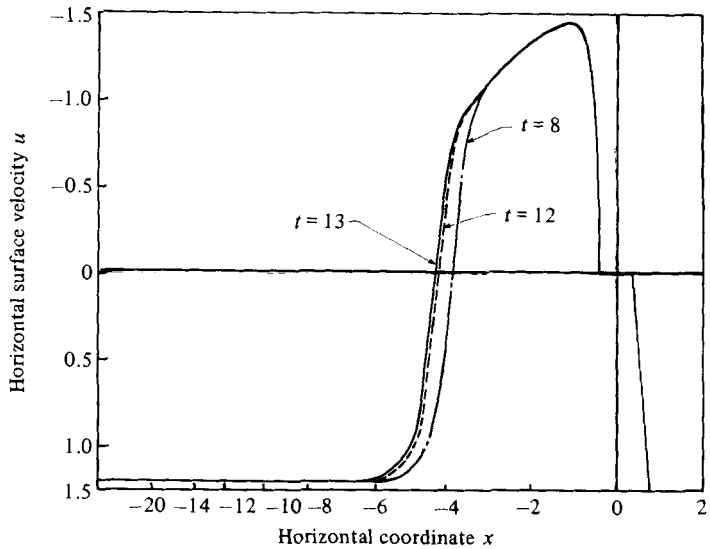

FIGURE 13. Horizontal velocity along the length of the flow region of the free surface ($z = 1$) and various time steps for the overflow case 10 ($F_s = 0.175$, $Re = 20$, $Q_s = 0.2$): Approach to equilibrium.

of the interface identified by the $\gamma = 0.1\gamma_e$ isopycnic with the dividing streamline $\psi = 0.8$. Because $\psi = 0.8$ is below $\gamma = 0.1\gamma_e$, some of the source fluid was entrained into the lower layer. If we examine figure 9(*a*), we may observe for case 4 the location of the $\psi = 0.8$ streamline in relation to the $\gamma = 0.1\gamma_e$ isopycnic. This streamline is below the upstream current; therefore, downward entrainment occurs in that case as well. However, for the near-critical case (case 8), presented in figure 6, upward entrainment across the upstream front occurs since the dividing streamline is above the $\gamma = 0.1\gamma_e$ isopycnic, viz the isopycnic that identifies the frontal boundary. For the other computed cases close to the critical case, upward entrainment was predicted as well. Therefore we observe that the entrainment direction is not necessarily one-sided but depends upon the properties of the flowfield. Upward entrainment tends to occur for small values of F_s, while downward entrainment tends to occur for large values of F_s.

Figure 12(*b*) is a photograph of a laboratory-produced upstream intrusion with a streamwise Froude number equal to approximately 0.02 and a source-densimetric Froude number squared F_s^2 equal to approximately 0.02. This experiment is relatively close to case 9. Qualitative agreement of the shape of the surface layers can be observed by comparing the shape of the $\gamma = 0.1\gamma_e$ isopycnic in figure 12(*a*) with the shape of the dyed surface in figure 12(*b*). The head, or frontal zone, is shallower than the following current in both the numerical solution and the experiment. Also, the depth of the following current in both cases is approximately equal to one-half the channel depth.

The intrusion process was initiated again to examine the final stage of zonal equilibrium for a larger Froude number. In addition, the upstream velocity profile was assumed to be a fully established shear flow with a parabolic shear profile. Therefore, bottom shear was also included. As expected, the deceleration was more rapid than in the other two cases (4 and 9). In this case (case 10) we concentrate on examining the near-equilibrium solutions, i.e. the solutions for $t > 8$. By this time the

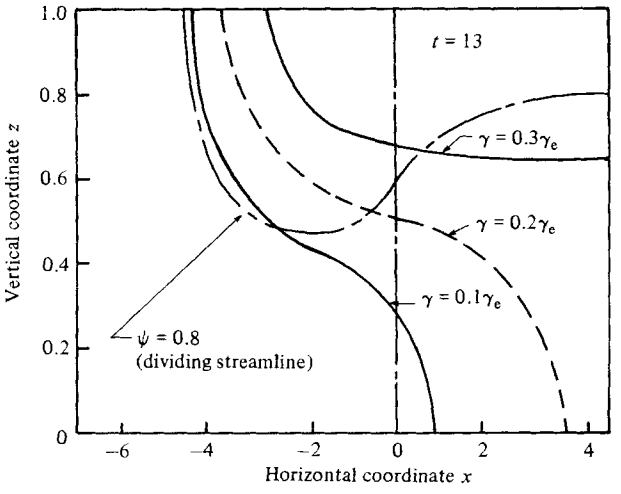

FIGURE 14. Isopycnic lines corresponding to $t = 13$ for the overflow case 10 ($F_s = 0.175$, $Re = 20$, $Q_s = 0.2$).

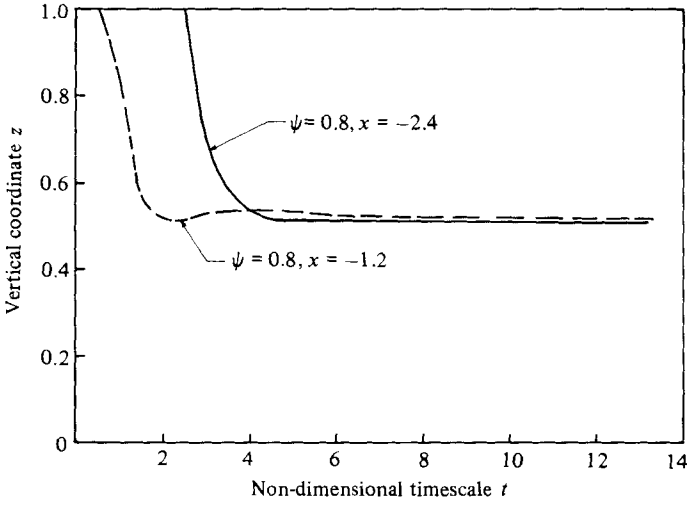

FIGURE 15. Depth of dividing streamline ($\psi = 0.8$) versus time at $x = -2.4$ and $x = -1.2$ for the overflow case 10 ($F_s = 0.175$, $Re = 2$, $Q_s = 0.2$): approach to equilibrium.

internal waves are damped significantly and the frontal region is propagating slowly upstream. The surface velocity profiles for the upstream intrusion are presented in figure 13.

The current behind the front has already reached a steady state in an analogous manner with the previous cases. The isopycnic contours and the dividing streamline for $t = 13$ are presented in figure 14. The bottom of the channel has affected the flow-field considerably, as indicated by the bottoming of the $\gamma = 0.1\gamma_e$ isopycnic. The strong upward entrainment in the following-current zone illustrates the enhanced mixing produced by the bottom shear. As already described, this enhances the deceleration process. For this case, the $\gamma = 0.1\gamma_e$ isopycnic identifies the front but not the interface of the following current. The $\gamma = 0.3\gamma_e$ remains horizontal, while the $\gamma = 0.1\gamma_e$ and the $\gamma = 0.2\gamma_e$ isopycnics extend to the bottom of the channel.

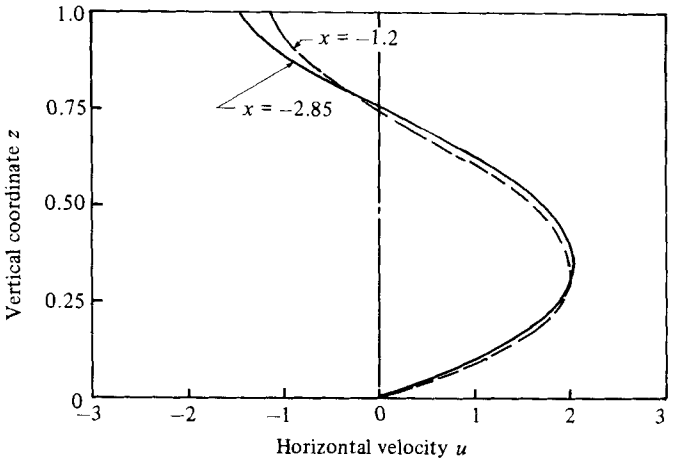

FIGURE 16. Steady-state horizontal velocity profiles behind the upstream front for case 10 ($F_s = 0.175$, $Re = 20$, $Q_s = 0.2$) at $x = -2.85$ and $x = -1.2$.

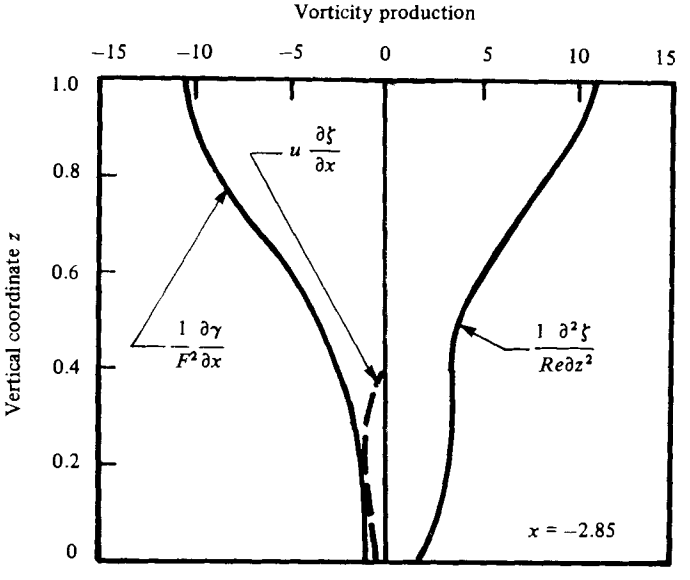

FIGURE 17. Balance of production of y-component of vorticity at $x = -2.85$ for case 10 ($F_s = 0.175$, $Re = 20$, $Q_s = 0.2$).

Figure 15 presents the time variation of the location below the surface of the 0.8 streamline, i.e. the dividing streamline. A steady state exists with respect to the inertial frame of reference in the layer of buoyant fluid behind the front. The steady-state velocity profiles at $x = -2.85$ and $x = -1.2$ confirm this; they are illustrated in figure 16. In the buoyant layer behind the front there is a balance between the production of vorticity caused by the nonhomogeneity of the density field and the diffusion of vorticity, i.e.

$$-\frac{1}{F^2}\frac{\partial \gamma}{\partial x} = \frac{1}{Re}\frac{\partial^2 \zeta}{\partial z^2} \tag{4.2}$$

(see figure 17). This result again illustrates the linear dynamics of the vorticity production in the surface layer. However, in the boundary layer below the buoyant layer the dynamics is decidedly nonlinear, with the advection of vorticity playing a role, i.e.

$$u\frac{\partial\zeta}{\partial x}=\frac{1}{F^2}\frac{\partial\gamma}{\partial x}+\frac{1}{Re}\frac{\partial^2\zeta}{\partial z^2}. \tag{4.3}$$

In summary, we examined the effects of Reynolds number, Froude number and bottom friction. In cases 4 and 9 a uniform flow far upstream of the source and pure-slip, zero-shear upper and lower boundary conditions were imposed. Therefore only the internal mixing (or interfacial shear) was altered by decreasing the Reynolds number for 200 to 20 going from case 4 to case 9 respectively. In case 10 the upstream velocity profile was assumed to be parabolic, the no-slip boundary condition was imposed at the channel bottom and the Froude number was increased in comparison to case 9. Therefore the effects of both bottom friction and ambient flow shear were computed and described.

The source-densimetric Froude number F_s is the principal parameter that defines the structure of an overflow of a buoyant effluent discharged into an open-channel flow. Upstream intrusions from the source location are possible when F_s is less than or equal to the critical value equal to about 0.85 (this assumes that the initial horizontal momentum of the buoyant overflow is negligible). When F_s is less than about 0.5 the upstream intrusion develops distinctly in four successive stages, viz initial acceleration, peak or plateau speed, deceleration and zonal equilibrium. The front accelerates toward the peak speed while the parent pool is increasing in depth. Once the effects of viscosity and entrainment intervene and the parent pool reaches its equilibrium depth, the upstream front decelerates. During the deceleration stage it oscillates at frequencies characteristic of internal gravity waves. As the front approaches its terminal velocity the waves are damped and the front moves slowly upstream.

A two-zone equilibrium is established when the front ceases to decelerate. In the frontal zone, the front propagates upstream at a steady velocity expanding the current zone following behind it. In the following current the flowfield reaches a steady state with respect to the inertial reference frame. In the overflow a balance is struck between the baroclinic production of vorticity and the vertical diffusion of vorticity. The velocity and density fields are stationary within the current region. Thus the vorticity dynamics is decidedly linear in the surface layer or gravity current behind the front. A criterion for defining the interface between the overflow and the receiving stream for the two-layered flow following the front is that the dividing line between the upper and lower layers is the line above which the vorticity production is linear.

Finally, the results of this investigation indicate that a totally arrested wedge is not possible; however, the intrusion tends towards such a state if the stream Froude number is sufficiently large. From a practical viewpoint a totally arrested wedge and a very slow-moving wedge in equilibrium are essentially equivalent. Also, recall that the gravity current behind the front approaches a steady, two-layered stratified flow; therefore it is not surprising that the experimental data reported in the literature (e.g. Bata 1957) on the geometry of the interface correlates with the Schijf & Schönfeld (1953) two-layered steady-flow model. It is from such a comparison that other researchers have concluded that the surface layers were arrested.

This work is based largely on the dissertation of the first author (DTV) presented in partial fulfillment of the requirements for the PhD degree at the Catholic University of America. The support of the U.S. National Science Foundation (NSF) under Grant NSF 77-01496 is gratefully acknowledged. The first author (DTV) also acknowledges the encouragement of his business associate and colleague Dr Bruce D. Cox, President of Hydrodynamics Research Associates Inc. The second author (TWK) also acknowledges the support of NSF under Grant CEE-83-08405.

REFERENCES

BATA, G. L. 1957 Recirculation of cooling water in rivers and canals. *J. Hydraul. Div. ASCE* **83** (HY3), 1–27 [*Proc. Paper* 1265].

BENJAMIN, T. B. 1968 Gravity currents and related phenomena. *J. Fluid Mech.* **31**, 209–248.

BRITTER, R. E. & SIMPSON, J. E. 1978 Experiments on the dynamics of a gravity current head. *J. Fluid Mech.* **88**, 223–240.

CEDERWALL, K. 1971 Buoyant slot jets into stagnant or flowing environments. *W. M. Keck Lab., California Inst. Tech., Rep.* KH-R-25.

DIDDEN, N. & MAXWORTHY, T. 1982 The viscous spreading of plane and axisymmetric gravity currents. *J. Fluid Mech.* **121**, 27–42.

GARVINE, R. W. 1974 Dynamics of small-scale oceanic fronts. *J. Phys. Oceanogr.* **4**, 557–569.

GARVINE, R. W. 1981 Frontal jump conditions for models of shallow, buoyant surface layer hydrodynamics. *Tellus* **33**, 301–311.

HUPPERT, H. E. 1982 The propagation of two-dimensional and axisymmetric viscous gravity currents over a rigid horizontal surface. *J. Fluid Mech.* **121**, 43–58.

KAO, T. W. 1977 Density currents and their applications. *J. Hydraul. Div. ASCE* **103** (HY5), 543–555 [*Proc. Paper* 12947].

KAO, T. W., PARK, C. & PAO, H.-P. 1978 Inflows, density currents and fronts. *Phys. Fluids* **21**, 1912–1922.

KÁRMÁN, T. VON 1940 The engineer grapples with non-linear problems. *Bull. Am. Math. Soc.* **46**, 615–683.

KEULEGAN, G. H. 1958 The motion of saline fronts in still water. *Natl Bur. Stand. Rep.* 5831.

LIN, Y. J. 1979 A study of inflow characteristics in a stratified fluid. PhD thesis, The Catholic University of America, Washington, D.C.

LUGT, H. & HAUSSLING, H. J. 1974 Laminar flow past an abruptly accelerating elliptic cylinder at 45° incidence. *J. Fluid Mech.* **65**, 711–734.

PAO, H.-P. & KAO, T. W. 1974 Dynamics of establishment of selective withdrawal of a stratified fluid from a line sink. Part 1. Theory. *J. Fluid Mech.* **65**, 657–688.

POLK, E. M., BENEDICT, B. A. & PARKER, F. L. 1971 Cooling water density wedges in streams. *J. Hydraul. Div. ASCE* **97** (HY10), 1639–1652.

ROACHE, P. J. 1972 *Computational Fluid Dynamics.* Hermosa.

SCHIJF, J. B. & SCHÖNFELD, J. C. 1953 Theoretical considerations on the motion of salt and fresh water. In *Proc. Minnesota Intl Hydraul. Convention, University of Minnesota.*

SIMPSON, J. E. 1972 Effects of the lower boundary on the head of a gravity current. *J. Fluid Mech.* **53**, 759–768.

SIMPSON, J. E. 1982 Gravity currents in the laboratory, atmosphere, and ocean. *Ann. Rev. Fluid Mech.* **14**, 213–234.

STIGEBRANDT, A. 1980 A note on the dynamics of small-scale fronts. *Geophys. Astrophys. Fluid Dyn.* **16**, 225–238.

TORRANCE, K. E. 1968 Comparison of finite-difference computations of natural convection. *J. Res. Natl Bur. Stand.* **B72**, 281–301.

TORRANCE, K. E. & ROCKETT, J. A. 1969 Numerical study of natural convection in an enclosure with localized heating from below: creeping flow to the onset of laminar instability. *J. Fluid Mech.* **36**, 33–54.